Available online at www.sciencedirect.com
ScienceDirect
Trans. Nonferrous Met. Soc. China 27(2017) 2214−2224
Transactions of Nonferrous Metals Society of China
www.tnmsc.cn

Constrained sintering and wear properties of Cu−WC composite coatings

J. L. CABEZAS-VILLA[1], L. OLMOS[2], H. J. VERGARA-HERNÁNDEZ[1],
O. JIMÉNEZ[3], P. GARNICA[1], D. BOUVARD[4], M. FLORES[3]

1. División de Estudios de Posgrado e Investigación, TecNM/Instituto Tecnológico de Morelia,
Av. Tecnológico #1500, Colonia Lomas de Santiaguito, Morelia, Michoacán, C. P. 58120, México;
2. INICIT, Universidad Michoacana de San Nicolás de Hidalgo,
Fco. J. Mujica S/N, Morelia, Michoacán, C. P. 58060, México;
3. Universidad de Guadalajara, Departamento de Ingeniería de Proyectos,
José Guadalupe Zuno # 48, Los Belenes, Zapopan, Jalisco, C. P. 45100, México;
4. Univ. Grenoble Alpes, CNRS, SIMaP, 38000 Grenoble, France

Received 26 October 2016; accepted 24 March 2017

Abstract: Coatings of metal matrix composites (Cu−WC) were fabricated by solid-state sintering. WC reinforcing particles in different quantities from 5% up to 30% (volume fraction) were mixed with Cu particles. After mixing, the powders were poured onto the surface of copper substrates. Sintering was carried out at 1000 °C under a reducing atmosphere in a vertical dilatometer. Sintering kinetics was affected by both rigid substrates and WC particles which retarded the radial and axial densification of powders. However, the coatings were strongly attached to the substrate, and WC particles were randomly distributed within the matrix. The addition of the reinforcing particles enhanced the microhardness and reduced the volume loss in wear tests to 1/17 compared to the unreinforced sample. The predominant wear mechanism was identified as abrasion at a load of 5 N. 20% WC (volume fraction) reinforcing particles led to the maximum values of properties for the composite coating.

Key words: constrained sintering; dilatometry; dry sliding wear; microhardness; metal matrix composites; coating

1 Introduction

Copper and its alloys have several automotive applications since they are efficient by combining multiple electrical, thermal and corrosion components. Nevertheless, the applications of copper alloys are often limited because of their low mechanical properties when compared to steel, aluminum or nickel. In particular, copper alloys are used to produce bearings in which a coating of powders is sintered onto a rigid substrate. In order to obtain a continuous process, the powders are poured onto the surface of the substrate; then, free sintering is achieved by introducing the products into an industrial furnace under a reducing atmosphere. Different problems are present during the process (e.g., delamination, large porosities, cracks), which are generated by the constrained sintering. Those problems reduce the life of bearings as well as the wear properties of the copper alloys. A few works have studied constrained sintering to fabricate coatings composed of powders on solid substrates [1−5]. Most of those works studied the sintering process and pointed out defects like pores and grain anisotropy [6] and delamination during sintering [7]. However, none of those works investigated the wear properties of the films. On the other hand, metal matrix composites reinforced with ceramic particles [8−11], whiskers [12] and nanoparticles [13,14] have been developed in order to improve the wear resistance and mechanical properties of different alloys. With respect to Cu alloys, DESHPANDE et al [15,16] observed that the pore volume and pore geometry increased the wear rate in composites of Cu−WC made by the infiltration process. HONG et al [17] found that small quantities of indium can improve the hardness and wear properties of the Cu−WC composites. LARIONOVA et al [18] introduced carbon nanofibers into a Cu matrix and reported that the coefficient of friction (CoF) was reduced up to 1/8 compared to that of the matrix. KHOSRAVI et al [19] used the stir process to

Corresponding author: L. OLMOS; E-mail: luisra24@gmail.com
DOI: 10.1016/S1003-6326(17)60247-4

fabricate layers of Cu−WC composites on solid substrates of copper; they found that the hardness was improved up to two times with respect to that of the pure copper, which was attributed to the reduction of the grain size. MIRAZIMI et al [20] fabricated composites of Cu−YSZ by SPS and obtained relative densities close to 95%, thus, microhardness and wear properties were improved. Nonetheless, the coefficient of friction was reported to be around the same values. PAK et al [21] produced Cu matrix composites reinforced with carbon nanotubes by extrusion process, improving the hardness of composites 4 times by adding 10% of nanotubes.

The objective of the present work is to investigate the sintering kinetics of the Cu−WC_p composite coatings fabricated by the powder metallurgy route and their mechanical properties and wear resistance. The effect of the volume fraction of the reinforcing particles, the pore volume and the sintering defects were evaluated and linked to the wear properties of the coating.

2 Experimental

In order to fabricate 1 mm-thick metal matrix composites (MMC) coatings, spherical copper powders with an average particle size of 23 μm (Fig. 1(a)) and tungsten carbide (WC) powders with an average particle size of 70 μm (Fig. 1(b)) were used as a matrix and the reinforcing particles, respectively. The reinforcing particles were added from 5% to 30% (volume fraction) into the Cu matrix. With the aim to obtain a random distribution of the WC particles, the powder mixture was poured into a plastic container; then, it was shaken for 30 min using a turbula. Two solid substrates of Cu were used: the first one consisted of cylinders with diameters of 8 mm and height of 14 mm were used to evaluate the sintering kinetics; the second one was a rectangular plate of 20 mm × 10 mm × 3 mm that was used for the wear tests. In the interest of fabricating the coating, substrates were placed inside a container with the same surface of the substrate. However, the thickness of the container was 1 mm larger than that of the substrate. The surface of the substrates was polished to eliminate external oxidation to avoid any interface problem during sintering. This space was filled with the powders that were poured onto the substrate. The powders were tapped in order to obtain a uniform distribution and to increase the green density of the coating. Finally, the outer surface was swept with a metallic plate to obtain a flatter surface. More details of the experimental set-up can be found elsewhere [5]. Immediately after the samples inside of the containers were introduced into a horizontal electrical furnace, they were heated at 450 °C for 30 min and a heating rate of 20 °C/min (under a reducing atmosphere of 10% H_2 and 90% N_2) to achieve adhesion between the particles and the solid substrate. Then, the samples were taken out of the containers with the coatings of powders attached to the surface of the substrate. Finally, sintering was carried out at 1000 °C with a heating rate of 25 °C/min for 1 h under a reducing atmosphere in two different instruments: a vertical dilatometer LINSEIS L75 to obtain the sintering kinetics and a horizontal furnace to produce larger samples used during the wear tests. The microstructure of the sintered coatings was analyzed by means of a Tescan Mira3 field emission scanning electron microscope (FESEM) using polished cross-sectional samples.

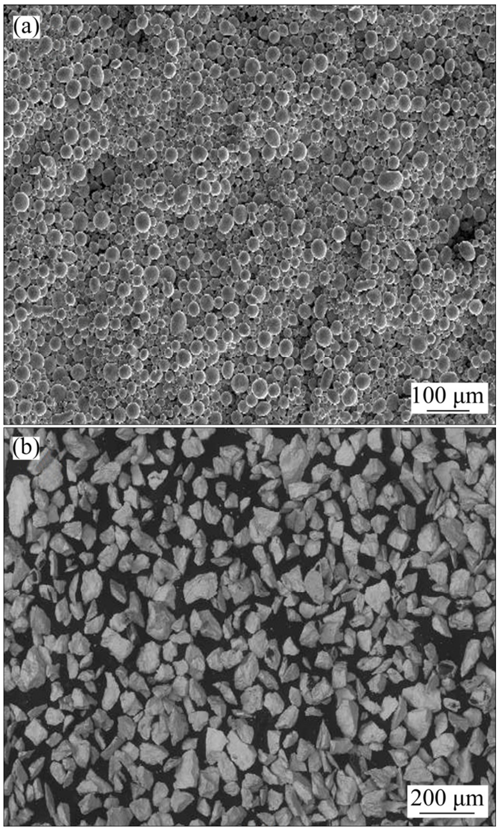

Fig. 1 FESEM images of initial powders: (a) Copper matrix; (b) WC used as inert inclusions

The microhardness evaluation was performed on cross-sectional polished surfaces by using a microhardness tester Mitutoyo MVK-HVL with a load of 0.5 N and a dwell time of 15 s. With the aim to obtain a map distribution of the microhardness, we indented in different locations on the coating surface from the interface with the substrate to the edge of the coating. A total of 49 points were measured and a 2D grid of 7×7 points was built; then, interpolation was performed using the Matlab software to obtain pseudo-continuous representations. Wear tests were performed at room temperature using a CETR UMT2 tribometer in a ball on flat, reciprocating sliding configurations under dry conditions and a relative humidity of 40%−45%. A

10-mm diameter AISI 52100 steel ball was used as the counterpart. Prior to starting the tests, the surface of the coatings was ground with SiC abrasive paper and then carefully polished with 1 μm particle size alumina. Finally, samples were ultrasonically cleaned in isopropyl alcohol and acetone for 15 min each. Every test was conducted with a sliding velocity of 0.02 m/s at a frequency of 1 Hz. The total number of cycles was chosen to be 1000 for the experiments, while the normal force was varied from 1 to 5 N. For every load, a new fresh surface was used to avoid any dust or contamination from previous runs. For each condition, three tests were made, and the average value was obtained. During testing, the round counterpart was kept stationary, while the working sample maintained the reciprocating sliding movement.

3 Results and discussion

3.1 Dilatometry analysis

The axial deformation during the whole thermal cycle undergone by the copper cylinder (used as a substrate) with and without a copper powder coating is shown in Fig. 2. The uncoated cylinder appears the dilation during the heating stage, which is due to the thermal expansion. Then, when the temperature reaches the isothermal plateau, no additional deformation is observed until the cooling stage starts. On the other hand, when the cylinder with the coating is evaluated, shrinkage starts at around 850 °C; this temperature corresponds to the sintering activation of copper powders, as it has been previously reported [22]. In this study, the shrinkage is associated to the coating of powders sintering on the surface of the cylinder. Shrinkage continues during the isothermal temperature, and when the cooling stage starts, the shrinkage corresponds to the thermal contraction.

In order to estimate the real shrinkage of the coating, the displacement measured by the dilatometer was corrected by the dilation of the copper cylinder at any temperature during the heating stage until the isothermal temperature was reached. Then, the shrinkage measured by the dilatometer corresponds exclusively to the dimensional changes on the coating. The real shrinkage of the coating was calculated by dividing the corrected displacement by the thickness of the coating composed of the powders. The shrinkage as a function of time during the isothermal sintering that was obtained for coatings with different volume fractions of reinforcing particles is depicted in Fig. 3. The level of shrinkage achieved is reduced when the volume fraction of WC particles increases. This behavior has been observed previously when the reinforcing particles are inert to the matrix at the sintering temperature [23]. The effect of the addition of WC particles on the axial shrinkage is important from 5% of WC particles that reduced 30% of the shrinkage reached by the coating without reinforcing particles. For the highest quantity of WC particles, the shrinkage is practically stopped, i.e., it is 92% lower than that obtained for the coating without reinforcing particles. It can also be observed that curves are not smoother than those reported for free sintering. This behavior can be attributed to a heterogeneous deformation of the coating due to the constraint generated by the substrate at the edges of the substrate, as was previously reported by GUILLON et al [1] and MARTIN and BORDIA [24]. That phenomenon is generated mainly because the center of the coating undergoes a higher shrinkage due to a stress concentration generated by the restriction of the substrate, which conserves its initial shape contrary to the powder that tries to shrink. Therefore, the possibility of delamination of the coating is higher at the edge of the substrate, where the necks developed between the

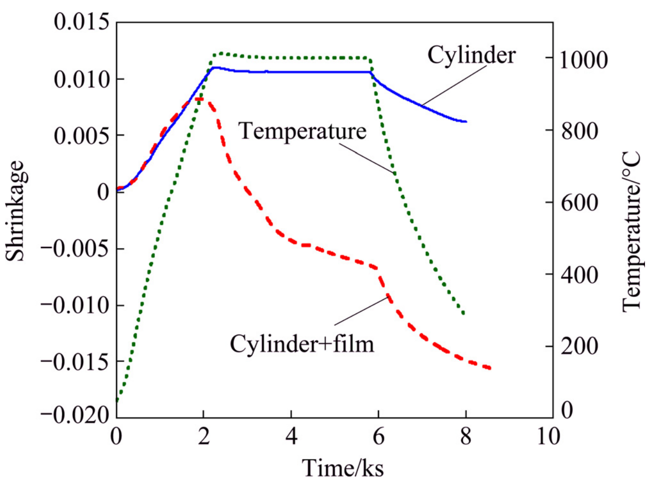

Fig. 2 Evolution of axial shrinkage as function of time during whole thermal cycle for substrate with and without coating

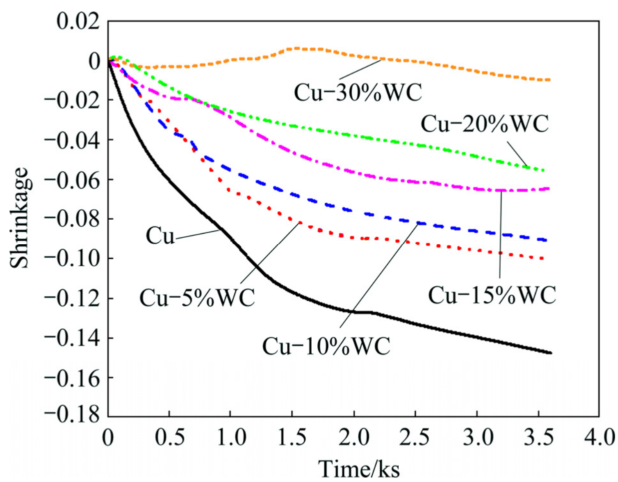

Fig. 3 Evolution of axial shrinkage as function of time on sintering plateau for coating with different volume fractions of reinforcing particles

particles and the flat surface of the substrate are weaker. These can be broken, especially for higher values of densification of powders as well as for coatings with smaller thicknesses. In this work, delamination was not detected since the maximum relative density attained was 82%, and the thickness of the coating is large enough to avoid inter-phase effects. However, a profile (in the form of a curvature) at the edge of the substrates for coatings without reinforcing and different zones of heterogeneous densification was observed. Different authors have also reported this curvature [25−27].

In order to estimate a global value of the relative density of the coatings, it was assumed that the radial deformation is zero; then, the final relative density was calculated from the dimensional changes measured by the dilatometer and the mass of powders used for the coating. Other authors have estimated the density from image analysis; however, as the copper is a soft material, some pores are filled during the polishing stage, and the relative density is overestimated. The relative density of coatings as a function of the volume fraction of WC particles is plotted in Fig. 4. We found a decrement of relative density when the reinforcing particles increased, which agrees with the shrinkage reduction by the addition of WC particles. During constrained sintering, the final relative density is similar to that reported for the free sintering for the same kind of composites [23]. These findings agree with those reported by LIN and JEAN [28] (the same relative density reached in this work: 80%) where a silver paste was sintered in both free and constrained sintering. In order to reach the same values of relative density for free and constrained sintering, the axial shrinkage should be higher for constrained sintering compared to that obtained by the free sintering since the radial densification is almost zero. Comparing the value of axial shrinkage for the same kind of composites obtained by free sintering reported by CABEZAS et al [23] and the shrinkage obtained by constrained sintering, the value is approximately 32% higher when constrained sintering is performed. On the other hand, different authors have pointed out that the constrained sintering inhibits the full densification via delamination, shape distortion, etc. However, those problems were seen in samples with relative densities above 90%, and there was a strong difference between constrained and free sintering; nevertheless, such densification is not achieved in this kind of coatings for bearing products because the remaining porosity helps to develop self-lubrication.

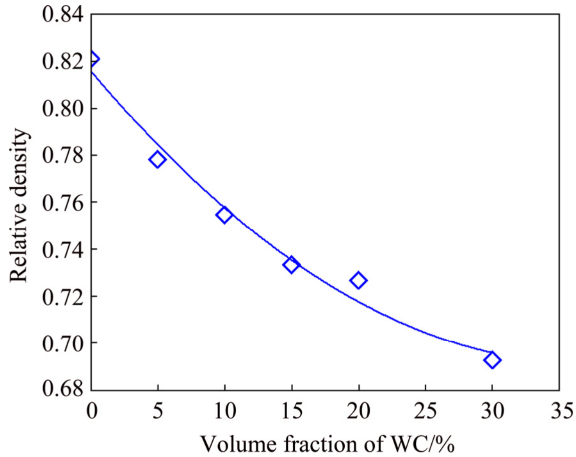

Fig. 4 Relative density of coatings as function of volume fraction of WC reinforcing particles

3.2 Microstructural observation

Figures 5 and 6 show cross-sectional FESEM images of the coatings processed by solid state sintering with and without WC reinforcing particles. In general, a residual porosity is noticed inside the coating (Fig. 5(a)). Also, larger pores can be seen as the volume fraction of the reinforcing particles increases (Fig. 5(f)). The rest of the samples show intermediate residual porosity. The WC particles are randomly distributed inside the Cu matrix. In spite of a good distribution of the particles,

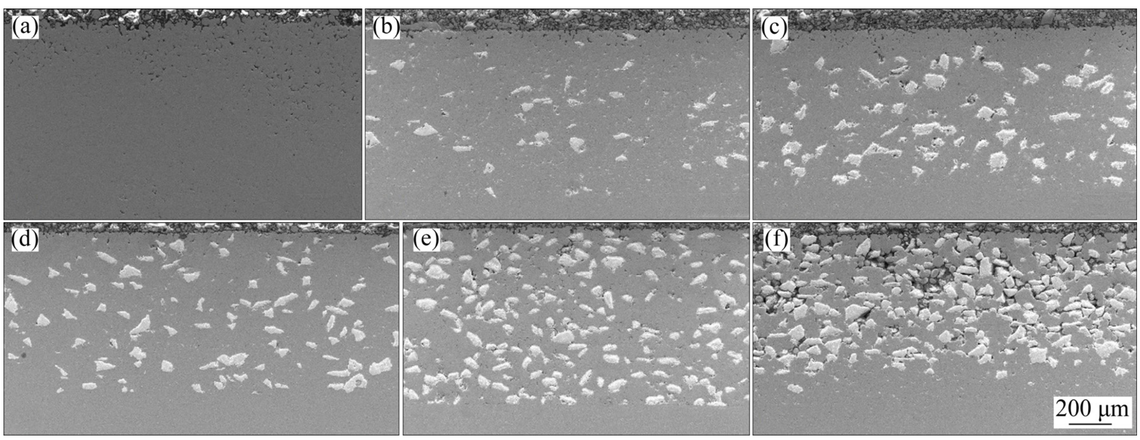

Fig. 5 FESEM images of composite films with different volume fractions of WC reinforcing particles: (a) 0; (b) 5%; (c) 10%; (d) 15%; (e) 20%; (f) 30%

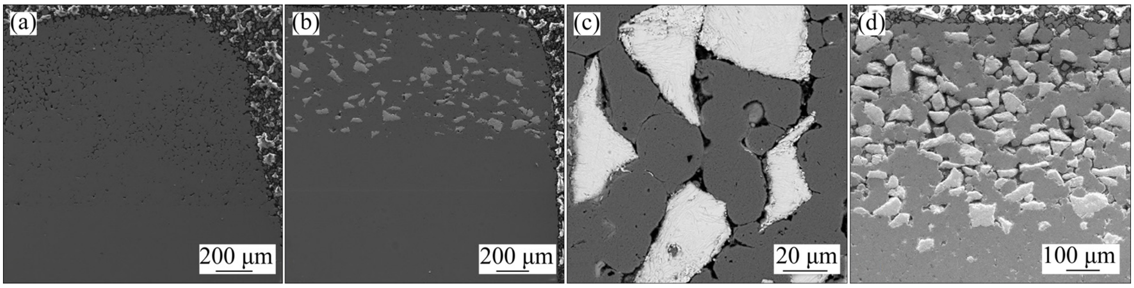

Fig. 6 FESEM images of composite films: (a) Edge of coating without WC particles; (b) Edge of coating with 10% WC particles; (c) Distribution of WC particles inside matrix sample with 15% WC particles; (d) Large agglomerates of WC particles (sample with 30% WC particles)

some zones are not denser than others because of the heterogeneous densification of powders, which is generated by the constraint imposed for the substrate, as it was also observed by other authors [3,5−7]. Particularly, denser zones are found at the edges of the coatings or for those with less than 20% WC particles. Above that quantity of WC particles, larger agglomerates are formed causing larger porosities. The inert behavior of the reinforcing particles is clearly observed in Fig. 6(c), where the WC particles are embedded in a continuous matrix. The continuity of the matrix is interrupted when 30% WC particles are added (Fig. 6(d)). A few Cu particles are sintered as isolated blocks and are surrounded by agglomerates of WC particles. This observation confirms the fact that the linear shrinkage detected by dilatometry is actually stopped.

3.3 Microhardness

In order to evaluate any favorable changes in the hardness of the composite coating, the average value of the matrix microhardness as a function of the volume fraction of the reinforcing particles is plotted in Fig. 7. Despite the relatively high dispersion of results, the microhardness increases by 25% for samples with volume fractions of WC particles up to 10%. Then, the microhardness increases as the volume fraction of WC particles increases and reaches a maximum value for samples with the volume fraction of WC particles of 20%. The maximum value is 60% higher than that for coating without any reinforcement. This value is 20% lower than that found by KHOSRAVI et al [19] in composite layers of Cu−WC fabricated by a stirring process. The same increment in hardness was reported by QIAN et al [29] for Cu−G composites with the same volume fraction of WS_2 reinforcing particles but fabricated by hot-pressing method. Finally, for the maximum volume fraction of WC particles used in this study, the microhardness values clearly decrease; however, this value is still 10% higher than that measured for coatings without inclusions. This behavior is consistent with that reported for the same system of metal matrix composites (Cu−WC); however, the threshold of inclusions was reported to be below 15%, and the maximum value of hardness was 75% higher than that obtained without inclusions in free sintering [23]. Higher values of hardness found in samples with inclusions indicate that the net of necks becomes stronger during sintering in spite of an increase in the porosity of the coatings.

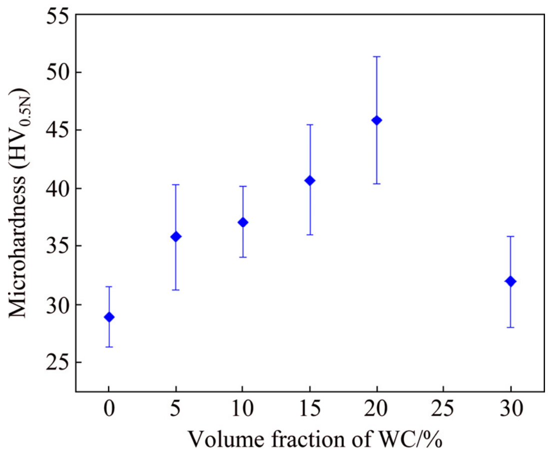

Fig. 7 Average values of microhardness as function of volume fraction of WC reinforcing particles

The microhardness distribution through the whole surface of coating is depicted in Fig. 8. The microhardness values increase with the increase of the volume fraction of WC particles, and they exhibit a maximum value for 20% WC reinforcing particles and a minimum value for 30% WC particles. The strengthening mechanisms of the matrix could be due to both: the effect of the transmission of load from the matrix to the inclusion particles and the mismatch in the coefficient thermal expansion (CET), which was described by CASATI and VEDANI [30]. The first one is attributed to the volume fraction of inclusions that have a higher stiffness than the matrix particles; thus, the charge is transmitted from the matrix to the WC particles when the matrix is completely interconnected. The second one is mainly because during cooling, the CTE is completely

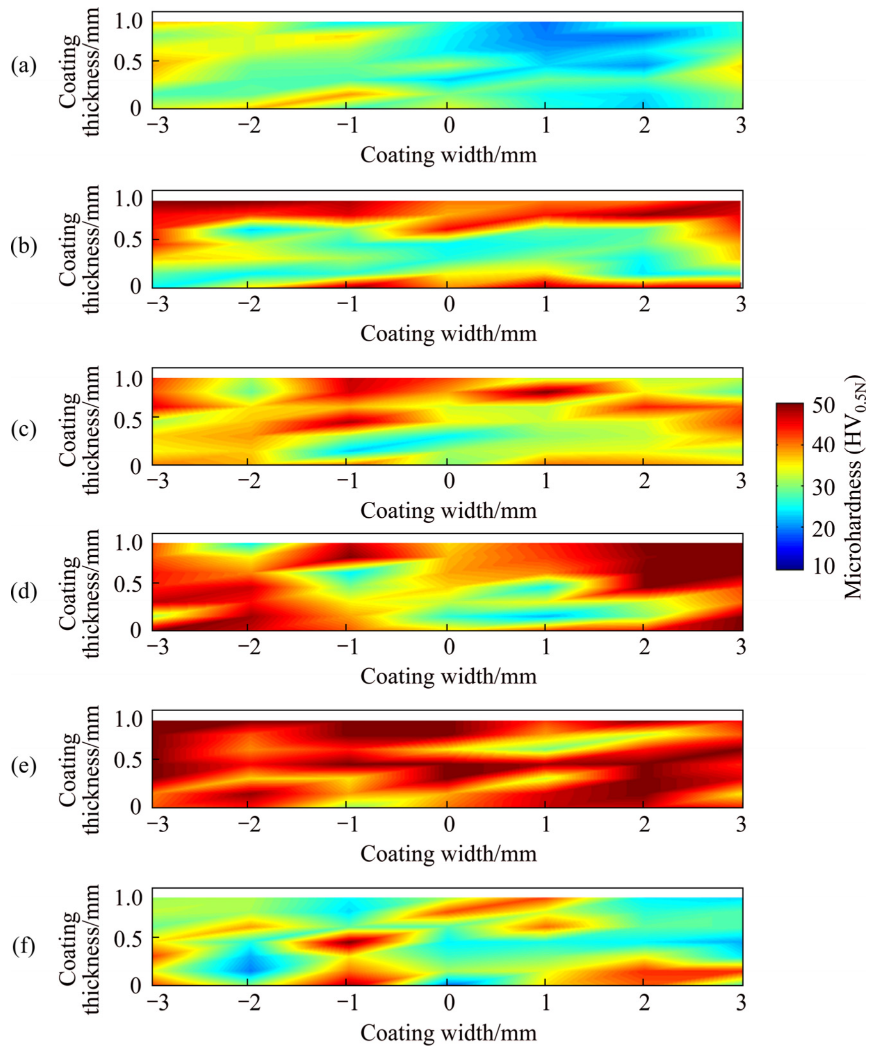

Fig. 8 Microhardness distribution on composite surface coatings with different volume fractions of WC reinforcing particles: (a) 0; (b) 5%; (c) 10%; (d) 15%; (e) 20%; (f) 30%

different between the matrix and the hard inclusions; therefore, internal stresses are generated in the matrix and cause hardening. Since the CTE is 3 times larger for the matrix than that for reinforcing particles, this mechanism should play a major role. These strengthening mechanisms are preponderant until the matrix is still interconnected, which means 20% of reinforcing particles. Above this quantity of WC particles, the lower densification plays a major role because larger pores are obtained and the continuity of the matrix is reduced. This reduction in matrix continuity mainly occurs because the reinforcing particles form a network between them, which inhibits further densification, as predicted by the percolation theory of LANGE et al [31,32] and as demonstrated by numerical simulations of bimodal compacts by BOUVARD and LANGE [33]. CABEZAS et al [23] found that 15% (volume fraction) of non-densifying particles is the threshold for reinforced composites fabricated by solid-state sintering. That value is in agreement with those reported by different authors [31−33]. Other authors have found that 20% (volume fraction) inclusions is the maximum quantity for the metal matrix composites of aluminium reinforced with SiC [8,9] and for ceramic matrix composites reinforced with nanoparticles [13]. However, the microhardness on the coating surface has also been observed to be highly heterogeneous, even when no WC particles are added. This result is consistent with the observations made regarding the porosity, which could be one of the causes of these heterogeneities [3,34]. Nonetheless, the microhardness of the matrix has been improved by the inclusion of WC particles, and the results show that 20% of hard inclusion gives more homogeneous hardness values through the evaluated area.

3.4 Dry sliding wear

The wear behavior of the Cu and Cu−WC coatings was evaluated in reciprocating sliding tests. This method has been used to evaluate the wear properties of thin coatings [35]. The evolution of the CoF of these samples as a function of the number of cycles at a load of 5 N is presented in Fig. 9. Similar behavior was found for samples tested with lower loads. Composites with 5% and 20% of reinforcement particles show relatively low CoF values around 0.25. The rest of the tested samples presented generally higher CoF values for the three loads used. It is not evident under which conditions of load or reinforcement the samples developed a steady friction coefficient as most of them showed different values when varying loads. With regard to the CoF values as a function of the reinforcement volume fraction, samples with reinforcements of 10% and above showed higher CoF values (with the exception of two conditions: 5 N, 5% WC and 5 N, 20% WC); however, as the volume fraction of WC increases for every used load, the dispersion of data is reduced. This is the result of a better distribution of the WC reinforcing particles inside the tested area. The CoF values found here are 1.5 times larger than those obtained in composites of Cu−WC fabricated by infiltration [15,17], clearly indicating that the way that the particles are embedded into the matrix and the differences during processing (in which there is at least one liquid phase) are the main causes from these results. On the other hand, the CoF values reported for composites fabricated by the stir process are slightly higher than those found here for the same quantity of WC particles being 10% (volume fraction) [19].

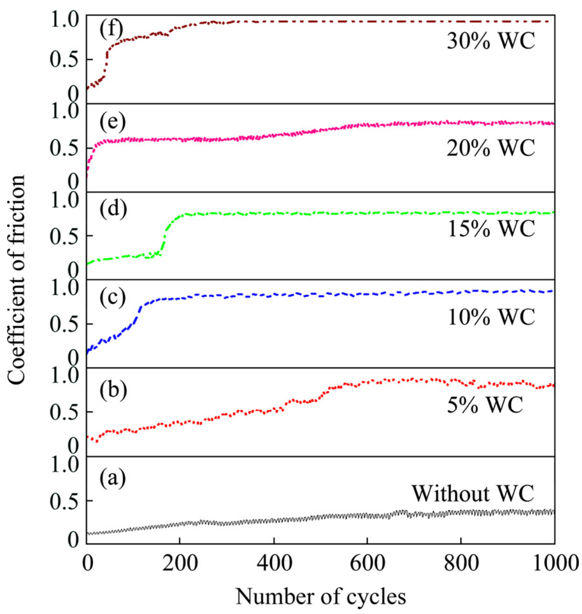

Fig. 9 Coefficient of friction as function of number of cycles for coatings with and without WC particles at load of 5 N

The volume loss for all tested samples as a function of volume fraction of WC particles for each load is presented in Fig. 10. In general, the volume loss, which is directly related to the wear rate, increases with the load for all samples except for the sample containing 20% of WC reinforcing particles. In this particular case, the sample shows a small increment for the intermediate load of 3 N; then, a slight decrement is again observed for the higher load. It has been previously reported [15] that one of the factors influencing loss of material in experiments with variation of the applied load is the local temperature reached on the worn surface of the sample. A high temperature is associated with a loss of interfacial strength between both phases (matrix and the reinforcement), which can originate loosening of the particle as well as removal. These results were found to be in agreement with the Archard wear law, which indicates that wear is proportional with the increase of applied load [36]. In other studies [15,37], an increased loss of material with the applied load was also reported.

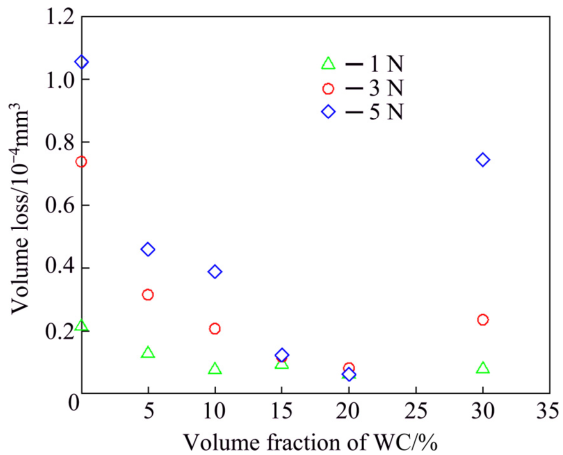

Fig. 10 Volume loss from reciprocating sliding tests as function of volume fraction of WC reinforcing particles at three different loads

The volume loss for the unreinforced sample is considerably higher than that of its counterpart which shows a reduction with a linear tendency as the volume fraction of reinforcing particles increases at a load of 1 N. Afterwards, higher loads of 3 and 5 N show a reduction of volume loss that behaves exponentially; this demonstrates that composites become more resistant to wear up to a reinforcing particle content of 20% (volume fraction). The reinforcing hard particles as a second phase can, in this case, act as a load carrier and impede the metal flow of the soft matrix; then, the removal of material is reduced. The importance of reinforcing particles in composites against wear has been previously reported in Refs. [38−40]. In this study, the volume loss is reduced to 1/17 for the sample with 20% of WC particles compared to the unreinforced sample at a load of 5 N.

In order to establish a relationship between the hardness of the coating and the volume loss under wear conditions, Archard's law [36] is useful to understand the compromise between both parameters, which describes the inverse relationship between these parameters (W and H), as shown in Eq. (1):

$$W = K\frac{LS}{H} \tag{1}$$

where W is the wear volume loss, K is the wear coefficient, L is the applied load, S is the sliding distance and H is the hardness of the softest contacting surfaces. With the aim to estimate the wear coefficient, the loss volume of each sample after 1000 cycles as a function of the inverse of the microhardness was plotted for samples tested at the same values of loads (Fig. 11). A linear behavior is seen for the three different loads used here. Also, the slope increases with the increase of the load, and the dispersion of values diminishes. On the other hand, the value of K was calculated from the slope of the linear fit for each set of points in Fig. 11. The K values obtained are 16.2×10^{-7}, 15×10^{-7} and 9×10^{-7} at loads of 5, 3 and 1 N, respectively. The value of K increases around two times from the lower load (1 N) to the higher load (5 N). This indicates that the conditions of the wear change with the applied load from light to severe. According to Archard's law, the wear undergone by these composites for higher loads should be abrasive.

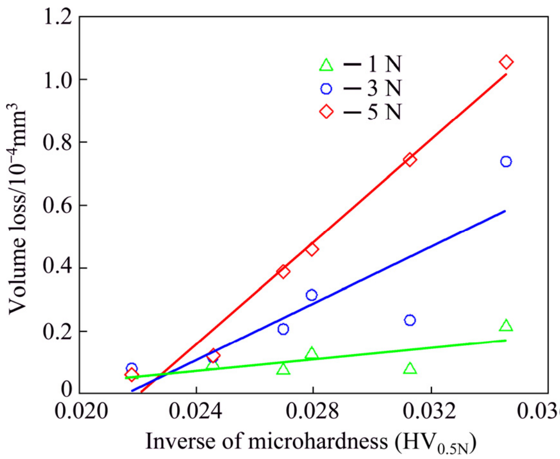

Fig. 11 Volume loss as function of inverse of microhardness for samples with and without WC reinforcing particles at different loads for reciprocating sliding tests

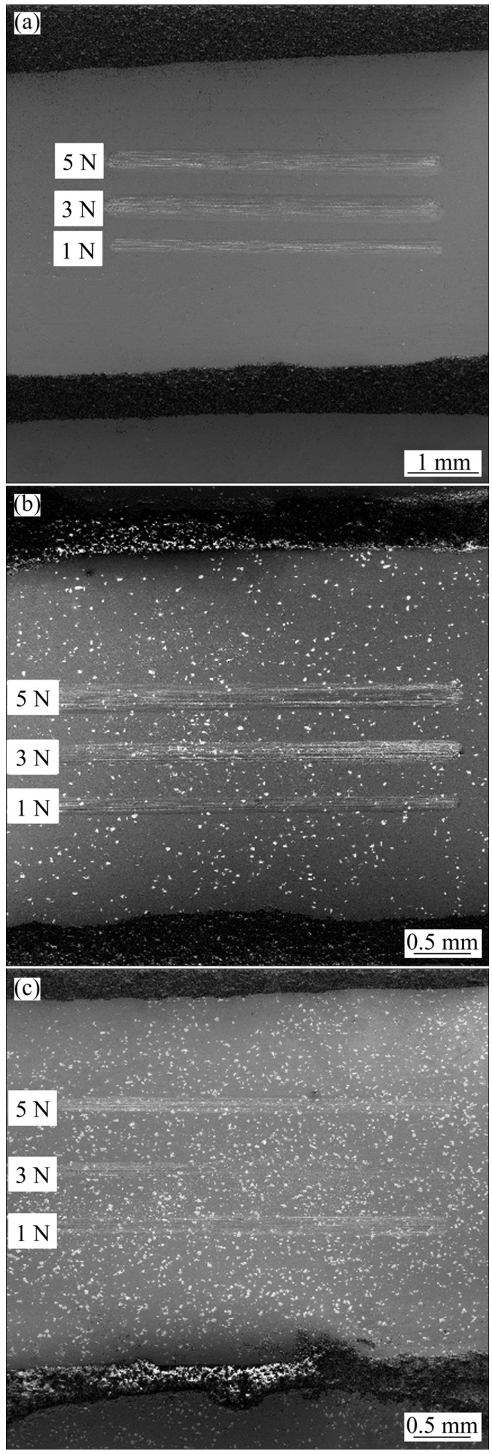

Fig. 12 FESEM images of wear scars at loads of 1, 3 and 5 N for three different samples: (a) Cu; (b) Cu−5%WC; (c) Cu−15%WC

3.5 Microstructural analysis of wear mechanisms

The worn surfaces after the tribological tests are presented in Figs. 12 and 13. It is observed that after sliding, the wear scars are smaller as the volume fraction of WC particles increases at different loads used (Fig. 12). These images also show that WC particles are randomly distributed over the coating surface and confirm the observations in the cross-sectional images presented in Fig. 5. Taking into account the sample with 5% of WC particles, it is clearly noticed that there are not many WC particles inside the wear scar compared to samples with, for instance, 15% of WC particles. This observation helps to explain the fact that the CoF increases for the sample with a higher volume of WC. It is evident that the contact between the metallic counterpart and a mostly metallic sample without or just5% WC results in a lower CoF (as a result of a metal-to-metal contact). The residual porosity also has an

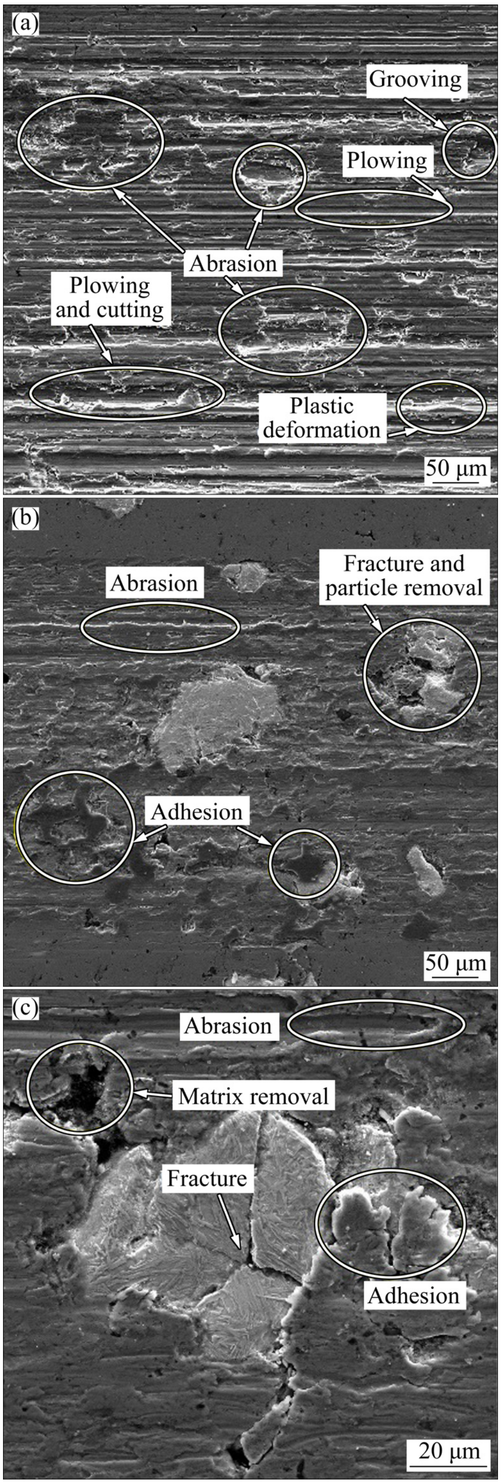

Fig. 13 FESEM images of worn surfaces for different loads and WC reinforcing particles: (a) Cu, 3 N; (b) Cu−15%WC, 3 N; (c) Cu−15%WC, 5 N

influence on the wear behavior of these composites. In this case, higher quantity of WC particles generate larger pores, which helps to reduce the volume loss. At first, the major wear occurred due to plastic deformation of the soft copper matrix that filled larger pores with matter removed from other places; this behavior was previously observed by MARTIN et al [41] in stainless steel porous samples.

In this study, the Cu matrix seems to be worn easily when no WC particles are used due to the low hardness of the Cu and the harder counterpart (Fig. 13(a)). This can also be associated with the size of the pores, which are relatively small; these cannot be easily filled by the removed material, and instead, growth occurs in the sliding direction. The wear mechanism identified at this stage can be described mainly as abrasive in which plowing, cutting, grooving and plastic deformation of the soft matrix are also seen. The removal material and the damage observed after sliding follow the statement that as being in different phases, composite components will respond individually to the wear events, which is mainly due to the difference in mechanical properties [38−40]. On the other hand, when WC particles are added to the Cu matrix, the volume loss decreases considerably up to a certain reinforcing particle content. Due to their hardness and load bearing capacity, they can better stand wear, while the remaining porosity is filled by the elimination of the asperities of the surface. Another reason for the decreasing volume loss is that the contact between the hard particles and the steel counterpart promotes the preferential wear of the soft Cu matrix. Previous studies [42,43] have shown that when the hardness of the counterpart (AISI 52100 in this case) is lower than that of the reinforcing particles, it is the matrix that wears preferentially, as seen in Fig. 13(b); although some abrasion is still seen, adhesion and removal of fractured WC particles are also observed. The interfacial bonding strength between WC particles and the Cu matrix resulted fairly good connection since only a few particles were either partly fractured or torn out from the matrix; thus, no other wear mechanisms than those previously described were identified, which is contrary to what has been found when Cu−WC composites are produced by the infiltration process [17]. The composites reinforced with WC particles (even when some of them can fracture, especially when higher loads are used) showed a reduced volume loss; also, the fractured particles tended to remain inside the matrix due to the bonding strength that was previously mentioned (Fig. 13(c)). From those images, it is estimated that the predominant wear mechanisms are both adhesive and abrasive with some material removal from the matrix.

4 Conclusions

1) Thick Cu-powder coatings were fabricated by solid-state sintering, and the effect of WC reinforcing particles on the wear properties was evaluated. Microhardness and dry reciprocating sliding wear tests

were carried out on samples with different volume fractions of WC particles.

2) The effect of substrate inhibited the radial densification during sintering, and delamination was not found because the final relative density attained is relatively low, which reduces the stress induced by densification of the powders on the substrate. The addition of WC particles acting as inert material at the sintering temperature slowed the densification of the coating when the volume fraction of WC particles increased in the same way reported by free sintering of composites.

3) The microhardness of the Cu matrix is improved by the addition of hard particles in spite of an increase on the porosity, and the optimum volume fraction of WC particles is 20%. The effect of increasing microhardness is positive for the wear behavior since the volume loss is reduced when the microhardness is increased, particularly for higher loads under which the reduction of volume loss follows an exponential behavior. A higher coefficient of friction was also found when hard particles were used, but a clear tendency was not observed when increasing the volume fraction of WC particles. The predominant wear mechanism was found to be abrasive (mainly for high loads), whereas adhesion may be present depending on experimental conditions. Finally, the reinforcing particles remained embedded within the Cu matrix since they were not completely torn off from the matrix due to its high bonding strength.

Acknowledgements

The authors would like to thank to CONACyT through the project CB-167111, the Scientific Research Department of the UMSNH and the Guadalajara University for the financial support and the facilities to develop this study.

References

[1] GUILLON O, KRAUß S, RÖDEL J. Influence of thickness on the constrained sintering of alumina films [J]. Journal of the European Ceramic Society, 2007, 27: 2623−2627.

[2] KIM J S, RUDKIN R A, WANG X, ATKINSON A. Constrained sintering kinetics of 3YSZ films [J]. Journal of the European Ceramic Society, 2011, 31: 2231−2239.

[3] BERNARD D, GUILLON O, COMBARET N, PLOUGONVEN E. Constrained sintering of glass films: Microstructure evolution assessed through synchrotron computed microtomography [J]. Acta Materialia, 2011, 59: 6228−6238.

[4] WALLOT J, REYNDERS P, HERZING A A, KIELY C J, HARMER M P, RÖDEL J. Sintering of thin film nanocrystalline titania–tin oxide composites [J]. Journal of the European Ceramic Society, 2008, 28: 2225−2232.

[5] OLMOS L, LEMUS-RUIZ J, VERGARA-HERNÁNDEZ H J, JIMENEZ O, SALGADO J M L, TENA-MARTINEZ J J. Characterization of constrained sintering of powders on solid substrate [J]. Materials Science Forum, 2014, 793: 135−141.

[6] AMARAL L, JAMIN C, SENOS A M, VILARINHO P M, GUILLON O. Constrained sintering of $BaLa_4Ti_4O_{15}$ thick films: Pore and grain anisotropy [J]. Journal of the European Ceramic Society, 2013, 33: 1801−1808.

[7] RASP T, JAMIN C, WONISCH A, KRAFT T, GUILLON O. Shape distortion and delamination during constrained sintering of ceramic stripes: Discrete element simulations and experiments [J]. Journal of the American Ceramic Society, 2012, 95: 586−592.

[8] GHOSH S K, SAHA P. Crack and wear behavior of SiC particulate reinforced aluminium based metal matrix composite fabricated by direct metal laser sintering process [J]. Materials and Design, 2011, 32: 139−145.

[9] LAKSHMIPATHY J, KULENDRAN B. Reciprocating wear behavior of 7075Al/SiC in comparison with 6061Al/Al_2O_3 composites [J]. International Journal of Refractory Metals and Hard Materials, 2014, 46: 137−144.

[10] XIAO H, SHIN Y, LI P, SUE H J, LIANG H. A new composite designed to resist wear [J]. Materials and Design, 2014, 63: 749−756.

[11] ZHAO N, LI J, YANG X. Influence of the P/M process on the microstructure and properties of WC reinforced copper matrix composite [J]. Journal of Materials Science, 2004, 39: 4829−4834.

[12] LIANG Y N, LEE S W, PARK D S. Effects of whisker distribution and sintering temperature on friction and wear of Si3N4-whisker-reinforced Si3N4-composites [J]. Wear, 1999, 225−229: 1327−1337.

[13] KIM S W, KHALIL K A, COCKCROFT S L, HUI D, LEE J H. Sintering behavior and mechanical properties of HA−X% mol 3YSZ composites sintered by high frequency induction heated sintering [J]. Composites (Part B): Engineering, 2013, 45: 1689−1693.

[14] BATHULA S, SARAVANAN M, DHAR A. Nanoindentation and wear characteristics of Al 5083/SiC_p nanocomposites synthesized by high energy ball milling and spark plasma sintering [J]. Journal of Materials Science and Technology, 2012, 28: 969−975.

[15] DESHPANDE P K, LIN R Y. Wear resistance of WC particle reinforced copper matrix composites and the effect of porosity [J]. Materials Science and Engineering A, 2006, 418: 137−145.

[16] DESHPANDE P K, LI J H, LIN R Y. Infrared processed Cu composites reinforced with WC particles [J]. Materials Science and Engineering A, 2006, 429: 58−65.

[17] HONG E, KAPLIN B, YOU T, SUH M S, KIM Y S, CHOE H. Tribological properties of copper alloy-based composites reinforced with tungsten carbide particles [J]. Wear, 2011, 270: 591−597.

[18] LARIONOVA T, KOLTSOVA T, FADIN Y, TOLOCHKO O. Friction and wear of copper–carbon nanofibers compact composites prepared by chemical vapor deposition [J]. Wear, 2014, 319: 118−122.

[19] KHOSRAVI J, GIVI M K B, BARMOUZ M, RAHI A. Microstructural, mechanical, and thermophysical characterization of Cu/WC composite layers fabricated via friction stir processing [J]. International Journal of Advanced Manufacturing Technology, 2014, 74: 1087−1096.

[20] MIRAZIMI J, ABACHI P, PURAZRANG K. Microstructural characterization and dry sliding wear behavior of spark plasma sintered Cu−YSZ composites [J]. Transactions of Nonferrous Metals Society of China, 2016, 26: 1745−1754.

[21] PAK Ji-hun, KIM Gwi-nam, HWANG Sung-gu, KIM Beom-su, NOH Jung-pil, HUH Sun-chul. Mechanical properties of Cu matrix composite fabricated by extrusion process [J]. Transactions of Nonferrous Metals Society of China, 2016, 26(10): 2679−2686.

[22] OLMOS L, MARTIN C L, BOUVARD D. Sintering of mixtures of powders: Experiments and modelling [J]. Powder Technology, 2009, 190: 134−140.

[23] CABEZAS J L, OLMOS L, VERGARA-HERNÁNDEZ H J, GARNICA P, JIMÉNEZ O, MONDRAGÓN-SÁNCHEZ M L, LEMUS-RUIZ J. Investigation of the effect of inert inclusions on densification during solid-state sintering of metal matrix composites

[J]. Science and Engineering of Composite Materials, 2017, 24: 755−763.

[24] MARTIN C L, BORDIA R K. The effect of a substrate on the sintering of constrained films [J]. Acta Materialia, 2009, 57: 549−558.

[25] GREEN D J, GUILLON O, RÖDEL J. Constrained sintering: A delicate balance of scales [J]. Journal of the European Ceramic Society, 2008, 28: 1451−1466.

[26] MARTIN C L, CAMACHO-MONTES H, OLMOS L, BOUVARD D, BORDIA R K. Evolution of defects during sintering: Discrete element simulations [J]. Journal of the American Ceramic Society, 2009, 92: 1435−1441.

[27] JAMIN C, RASP T, KRAFT T, GUILLON O. Constrained sintering of alumina stripe patterns on rigid substrates: Effect of stripe geometry [J]. Journal of the European Ceramic Society, 2013, 33: 3221−3230.

[28] LIN Y C, JEAN J H. Constrained sintering of silver circuit paste [J]. Journal of the American Ceramic Society, 2004, 87: 187−191.

[29] QIAN Gang, FENG Yi, CHEN Yang-ming, MO Fei, WANG Yu-qing, LIU Wen-hong. Effect of WS_2 addition on electrical sliding wear behaviors of Cu–graphite–WS_2 composites [J]. Transactions of Nonferrous Metals Society of China, 2015, 25: 1986−1994.

[30] CASATI R, VEDANI M. Metal matrix composites reinforced by nano-particles—A review [J]. Metals, 2014, 4(1): 65−83.

[31] LANGE F F. Constrained network model for predicting densification behavior of composite powders [J]. Journal of Materials Research, 1987, 2: 59−65.

[32] LANGE F F, ATTERAAS L, ZOK F, PORTER J R. Deformation consolidation of metal powders containing steel inclusions [J]. Acta Metallurgica et Materialia, 1991, 39: 209−219.

[33] BOUVARD D, LANGE F F. Relation between percolation and particle coordination in binary powder mixtures [J]. Acta Metallurgica et Materialia, 1991, 39: 3083−3090.

[34] QI S, ZUO R, MA Z. Densification kinetics and anisotropic microstructure evolution in LTCC films constrained by rigid substrate [J]. Ceramics International, 2016, 42: 3388−3396.

[35] AGEH V, CHOUDHURI D, SCHARF T W. High frequency reciprocating sliding wear behavior and mechanisms of quaternary metal oxide coatings [J]. Wear, 2015, 330: 390−399.

[36] ARCHARD J F. Contact and rubbing of flat surfaces [J]. Journal of Applied Physics, 1953, 24: 981−988.

[37] DINAHARAN I, MURUGAN N. Dry sliding wear behavior of AA6061/ZrB_2 in-situ composite [J]. Transactions of Nonferrous Metals Society of China, 2012, 22: 810−818.

[38] JIANG X S, WANG N J, ZHU D G. Friction and wear properties of in-situ synthesized Al_2O_3 reinforced aluminum composites [J]. Transactions of Nonferrous Metals Society of China, 2014, 24: 2352−2358.

[39] RAMESH C S, AHAMED A. Friction and wear behaviour of cast Al6063 based in situ metal matrix composited [J]. Wear, 2011, 271: 1928−1939.

[40] YANG B, SUN M, GAN G, XU C, HUANG Z, ZHANG H, FANG Z Z. In situ Al_2O_3 particle reinforced Al and Cu matrix composites synthesized by displacement reactions [J]. Journal of Alloys and Compounds, 2010, 494: 261−265.

[41] MARTIN F, GARCÍA C, BLANCO Y. Influence of residual porosity on the dry and lubricated sliding wear of a powder metallurgy austenitic stainless steel [J]. Wear, 2015, 328−329: 1−7.

[42] COLACO R, VILAR R. Abrasive wear of metallic matrix reinforced materials [J]. Wear, 2003, 225: 643−650.

[43] ZUM GAHR K H. Wear by hard particles [J]. Tribology International, 1998, 31: 587−596.

Cu−WC 复合材料涂层的受限烧结和磨损性能

J. L. CABEZAS-VILLA[1], L. OLMOS[2], H. J. VERGARA-HERNÁNDEZ[1],
O. JIMÉNEZ[3], P. GARNICA[1], D. BOUVARD[4], M. FLORES[3]

1. División de Estudios de Posgrado e Investigación, TecNM/Instituto Tecnológico de Morelia,
Av. Tecnológico # 1500, Colonia Lomas de Santiaguito, Morelia, Michoacán, C. P. 58120, México;
2. INICIT, Universidad Michoacana de San Nicolás de Hidalgo,
Fco. J. Mujica S/N, Morelia, Michoacán, C. P. 58060, México;
3. Universidad de Guadalajara, Departamento de Ingeniería de Proyectos,
José Guadalupe Zuno # 48, Los Belenes, Zapopan, Jalisco, C. P. 45100, México;
4. Univ. Grenoble Alpes, CNRS, SIMaP, 38000 Grenoble, France

摘　要：采用固态烧结法制备 Cu−WC 金属基复合材料涂层。将不同体积分数(5%−30%)的 WC 增强颗粒与 Cu 颗粒混合，然后在还原性气氛和垂直膨胀计中于 1000 °C 进行烧结。结果表明，复合材料涂层的烧结动力学受基体材料和 WC 颗粒的影响，WC 颗粒能减缓粉末径向和轴向的致密化。复合材料涂层紧实地粘附于基体上，而 WC 颗粒随机分布在基体中。与未添加增强剂的样品相比，添加了 WC 增强剂的样品的显微硬度增加，磨损量降低至原来的 1/17。样品在载荷为 5 N 条件下的主要磨损机理为磨粒磨损，当 WC 增强剂的体积分数为 20%时复合涂层的性能最优。

关键词：受限烧结；膨胀法；干滑动磨损；显微硬度；金属基复合材料；涂层

(Edited by Wei-ping CHEN)